AIMS Materials Science, 4(4): 905-919.
DOI: 10.3934/matersci.2017.4.905
Received: 01 May 2017
Accepted: 19 July 2017
Published: 25 August 2017

http://www.aimspress.com/journal/Materials

Short review

Fabrication and applications of self-assembled nanopillars

Hai-Feng Ji [1,*], Morasae Samadi [1,2], Hao Gu [1], Veronica Tomchak [1], and Zhen Qiao [1]

[1] Department of Chemistry, Drexel University, Philadelphia, PA 19104, USA
[2] Institute for Nanoscience and Nanotechnology (INST), Sharif University of Technology, Tehran, Iran, 1667759318

*** Correspondence:** Email: hj56@drexel.edu; Tel: 01-215-895-2562; Fax: 01-215-895-1265.

Abstract: In this mini-review, we summarize fabrication methods, formation mechanisms, factors that control the characteristics, and applications of self-assembled nanopillars. Nanopillars prepared both in the gas phase and in solutions are discussed.

Keywords: self-assembly; nanopillar

1. Introduction

At the nanoscale, materials have distinctly different characteristics from their corresponding one at macroscopic scale. This is one of the main causes of the fast growth of research studies on nanomaterials in recent years. However, the key to achieving their applications for devices is the integration of the nanomaterials on desired locations of the devices. The two major strategies in coupling nanomaterials on surfaces are through the formation of multilayer of nanomaterials or through the formation of vertically nanostructures, such as nanopillars, i.e., nanowires standing on surfaces. In recent years, fabrication and applications of nanopillars have attracted more and more attention. There are two principle approaches to nanopillar fabrication: top-down approaches such as lithography and etching, and bottom-up growth techniques. Bottom-up fabrication methods of nanopillars include chemical vapor deposition (CVD) [1], physical vapor deposition (PVD) [2], template synthesis [3,4], and self-assembled methods. In this mini-review, we intend to summarize fabrication methods, formation mechanisms, factors controlling characteristics, and applications of nanopillars based on the bottom-up, self-assembly approach, with more attention being focused on the factors that affect the growth of the nanopillars. Top-down fabrications [5,6], including lithography based on templated methods [7,8], are not included in this short review. It is noteworthy

that although, to a certain extent, CVD and PVD belong to the self-assembled class of approaches and have been widely used to make nanopillars, such as nanopillars of ZnO, CdS, etc., we will only briefly summarize the reports which mentioned the concept of self-assembly. The purpose of this review is to provide new researchers in this area with a quick overview on the body of work containing self-assembled nanopillars. For reviews on nanopillars from CVD or PVD, readers are suggested to read other recent reviews [9–12].

2. Fabrication Methods and Formation Mechanisms

The self-assembly approach offers a simple and efficient method for growth aligned nanostructures. This includes:

a. Self-assembled inorganic nanopillars in the gas phase by deposition of aerosol, and pulsed laser deposition (PLD).
b. Self-assembled inorganic nanopillars in solutions by hydrothermal + polymer assisted template.
c. Self-assembled organic compounds in solution on surfaces through liquid evaporation.

2.1. Self-assembled Inorganic Nanopillars in the Gas Phase by Deposition of Aerosol or Pulsed Laser Deposition (PLD)

Both horizontal and vertical films can be formed on a substrate by deposition of aerosol in the gas phase. The vertical nanopillared films offer advantages over the horizontal ones when a larger surface area is required [13,14].

Lebedev et al. reported [15] nanopillared $(La_{0.67}Ca_{0.33}MnO_3)_{1-x}$:$(MgO)_x$ (LCMO) composite films on a MgO substrate. The films were prepared via the deposition of metal organic aerosols on the MgO substrate. The magneto-transport responses of the film depend on the percentage of (100) MgO in the composite ($0 < x < 0.8$) (Figure 1 left). The resistivity of the film increased dramatically when $x > 0.3$ due to its unique structure. The film was made of LCMO materials, with epitaxial nanopillars of MgO embedded in the LCMO film. The formation mechanism was proposed as shown in Figure 1 right.

In a later work, Moshnyaga et al. further confirmed the formation of vertical nanopillars made of a composition of $(La_{0.7}Ca_{0.3}MnO_3)_{1-x}$:$(MgO)_x$ [16]. Again, the magneto-transport properties of the nanopillared films could be tuned via the MgO components.

In later reports, the pulsed laser deposition (PLD) method becomes the most popular method in this area and it has been successfully used in the fabrication of ceramic materials with nanopillars embedded in films. PLD is a thin film deposition technique. The energy of laser beam is high enough to vaporize a material into a plasma and deposits the plasma on a substrate to form a thin film. A variety of materials, such as La_2O_3, $MnCO_3$, $SrCO_3$, ZnO, Bi_2O_3, Fe_2O_3 and Sm_2O_3, $BiFeO_3$:Sm_2O_3, $BiFeO_3$:$NiFe_2O_4$, $BaTiO_3$:$CoFe_2O_4$, $La_{0.5}Sr_{0.5}CoO_3$:$Ce_{0.9}Gd_{0.1}O_{1.95}$, etc, have been deposited on substrates to form vertical pillars with unique functionalities [17]. To name a few examples, Li et al. [18] prepared self-assembled $PbTiO_3$–$CoFe_2O_4$ epitaxial nanostructures on $SrTiO_3$ single crystals from a composite $0.67PbTiO_3$–$0.33CoFe_2O_4$ target by using the PLD approach. The nanostructures on the $SrTiO_3$ surface is composed of vertical columns of $CoFe_2O_4$ embedded in a $PbTiO_3$ film. In their later work [19], they also demonstrated multiferroic $xCoFe_2O_4$–$(1-x)PbTiO_3$ films on the same substrates.

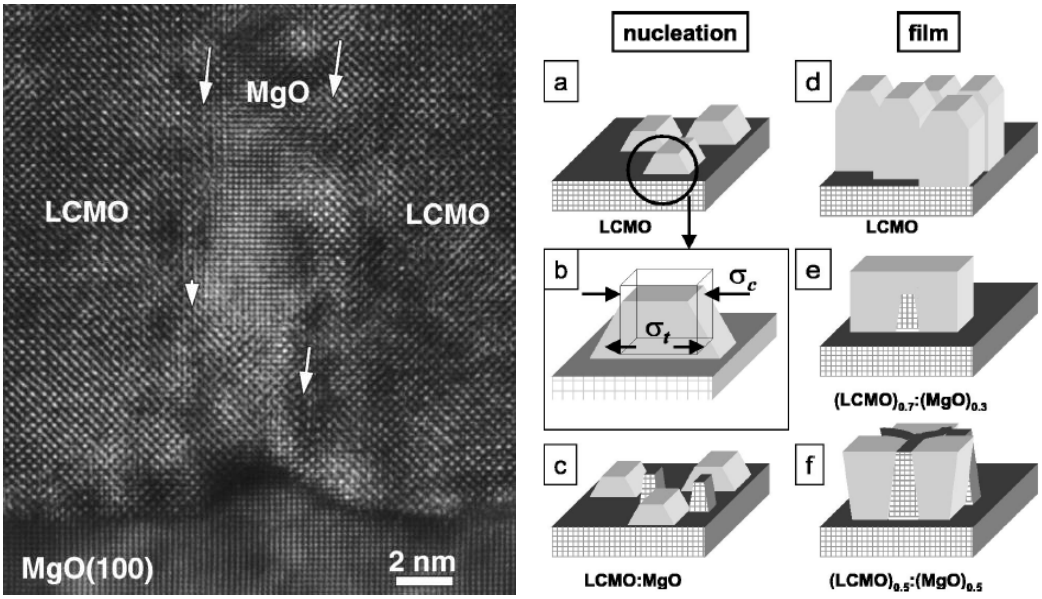

Figure 1. Left: Cross-section electron microscopy image of the interface $(La_{0.67}Ca_{0.33}MnO_3)_{1-x}$–$(MgO)_x$/MgO(100) for x = 0.5. Right: Schematic representation of the growth mechanism of the composite film at different stages: (a) Nucleation of the LCMO film on the MgO substrate. (b) Enlargement of one LCMO island on the MgO substrate. Close to the interface the LCMO region is under a two-dimensional tensile stress; the upper part of the LCMO island is under a two-dimensional compressive stress. The shape of LCMO becomes pyramidal. (c) Nucleation of the $(LCMO)_{1-x}$:$(MgO)_x$ composite film on the MgO substrate. (d) The columnar structure of the LCMO film on the MgO substrate. (e) Structure of the $(LCMO)_{1-x}$:$(MgO)_x$ film for x = 0.33. Intergrowth of the MgO islands in between LCMO domains occurs. (f) Structure of the $(LCMO)_{1-x}$:$(MgO)_x$ film for x = 0.5. Every LCMO grain is surrounded by MgO through the complete film thickness. Figure from Ref [15] reprinted with permission from the American Physics Society.

It has generally been accepted that the formation of the vertical nanostructures in films is due to the immiscibility of the two materials that requires the minimization of the interfacial and elastic strain energies between them. The morphology and the size of vertical nanopillars are related to the lattice misfit with the substrate [20]. By choosing two appropriate materials, nanopillar array can form in the epitaxial films. The properties of the films are related to the morphology and structure of the nanostructures and the interface. The two requirements for self-assembled two-phase nanocomposites are 1) the similarity of the crystal lattice parameters between the two materials; and 2) the low solubility or miscibility of the two materials. In the above paper, Li et al. [18] also showed orientation and morphology of the nanostructures could be controlled by the epitaxial stress of the substrates. The platelet-like column is parallel to the [110] and [111] planes for the [001] and [110] directions, respectively (Figure 2).

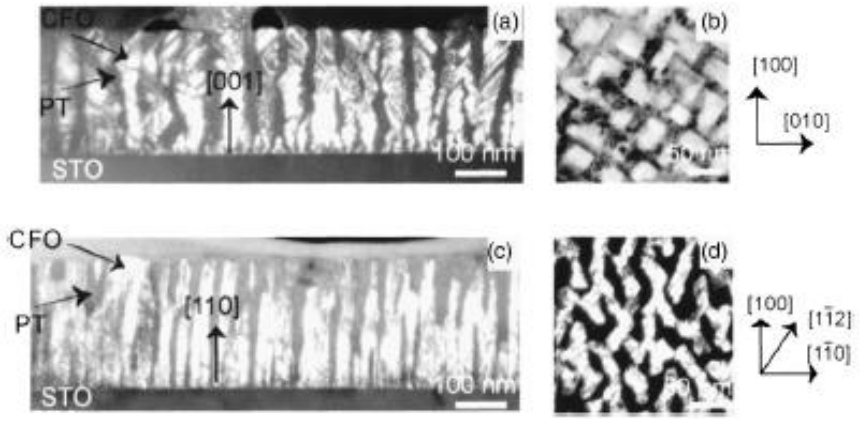

Figure 2. TEM images of the $PbTiO_3$–$CoFe_2O_4$ nanostructures grown on (001) $SrTiO_3$ (a) cross section, (b) plane view of the structures on (110) $SrTiO_3$. (c) cross section, (d) plane view the structures on (110) $SrTiO_3$. The image shown in (b) is a bright field image recorded near the [001] orientation parallel to the surface normal. In all the images, the $CoFe_2O_4$ phase appears as bright regions. Figure from Ref [18] reprinted with permission from the American Physics Society.

2.2. Self-assembled Inorganic Nanopillars in Solutions by Hydrothermal + Polymer Assisted Template

Deng et al. [21] developed self-assembled $(CoFe_2O_4)_{0.3}$–$(BaTiO_3)_{0.7}$ (CFO–BTO) feather-like nanopillars by using a cost-effective method that combined a hydrothermal reaction and a polymer-assisted fabrication. The crystalline CFO nanopillars were implanted in the BTO film. The mixed film showed unique ferromagnetic and ferroelectric properties. The proposed mechanism may be used for growing other perovskite-spinel nanomaterials.

By using a pulsed laser deposition method, Kim et al. prepared a three component self-assembled core-shell-matrix nanocomposite that was made of Cu nanorods that were covered by a shell of SrO embedded in a $Sr(Ti,Cu)O_{3-\delta}$ perovskite matrix on $SrTiO_3$ substrates [22]. After etching of Cu nanorods, the porous SrO pillars in the nanocomposite can be refilled with $CoFeO_4$ pillars in a $BiFeO_3$ perovskite matrix that showed unique magnetic properties.

2.3. Self-assembled Organic Compounds

Ji et al. have recently developed a novel, surface-assisted self-assembly approach to harvest vertically aligned single-crystalline organic nanopillar semiconductors from a solution of organic chemicals [23]. In these experiments, when cyanuric acid (CA) and melamine (M) are mixed at lower concentrations on a gold surface, an array of nearly 100% hexagonal nanopillars of the CA·M complex was obtained (scanning electron microscopy (SEM) images in Figure 3). The nanopillar is composed of a cyclic CA_3M_3 rosette assembly [24] (Figure 3 left). CA_3M_3 rosette molecular assemblies are hierarchically stacked or coordinated into insoluble nano- or micro-structures in 3D space due to hydrogen bonding, π–π stacking, hydrophobic interactions, and van der Waals interactions. They showed that the CA·M complexes nucleate as a thin, hexagonal plate on the gold surface at the onset stage, and grow wider and taller after more solvent evaporates. The unique aspect

of this result is that this assembly is the first of such well-defined self-assembled nanopillars made of small organic molecules. It is expected that arrays of pillars can be developed from several other complexes. The nanopillars prepared by this method can be made in large quantities at a low cost due to the facile self-assembling method. By using the same method, the group reported two self-assembled metal-organic micropillar arrays on Au surfaces: Cu/BTC prepared from Cu^{2+} and 1,3,5-benzenetricarboxylic acid (TBC), and Zn/ADC from Zn^{2+} and 9,10-anthracenedicarboxylic acid (ADC) [25,26].

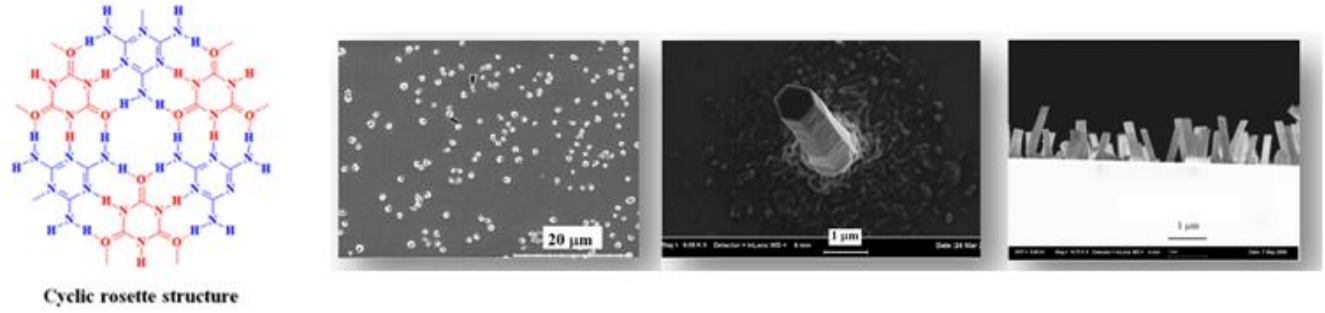

Figure 3. Molecular structures (left) and SEM images of 1:1 CA-M hexagonal nanopillars on a gold surface. Figure from Ref [23] reprinted with permission from the American Chemical Society.

Another organic nanopillar was prepared from a self-assembled mixture of copper phthalocyanine (CuPc) and 3,4,9,10-perylene-tetracarboxylic-dianhydride (PTCDA by using a thermal gradient sublimation technique [27,28]. The CuPc/PTCDA nanopillars may be used for developing organic photovoltaic cells and near-IR photodetectors. It is also interesting that polymers could form well-defined nanopillars by using a spin-casting process. These polymers should have large coplanar segments and strong attraction between polymers in order to self-assembling into nanopillars [29].

3. Factors Affecting the Growth and Characteristics of the Self-assembled Nanopillars

The property of surfaces is the main factor that controls the formation and characteristics of nanopillars. For the nanopillars from the pulsed laser deposition method, it has been believed that the growth of vertical nanopillars was due to the mismatch between the evaporated material and the substrate. This mismatch caused an in-plane compressive strain that limited the lateral growth of the material on the substrate [30]. The evaporated materials and substrates should have a similar structure and chemistry at their interface to facilitate the nucleation. This mechanism suggests that it is possible to design new nanostructures with desired properties by choosing appropriate substrates. For example, Zheng et al. [31] reported that the morphologies of self-assembled perovskite-spinel nanostructures were different on substrates with different orientations; rectangular $CoFe_2O_4$ nanopillars on a (001) and triangular $BiFeO_3$ nanopillars on a (111) substrate (Figure 4).

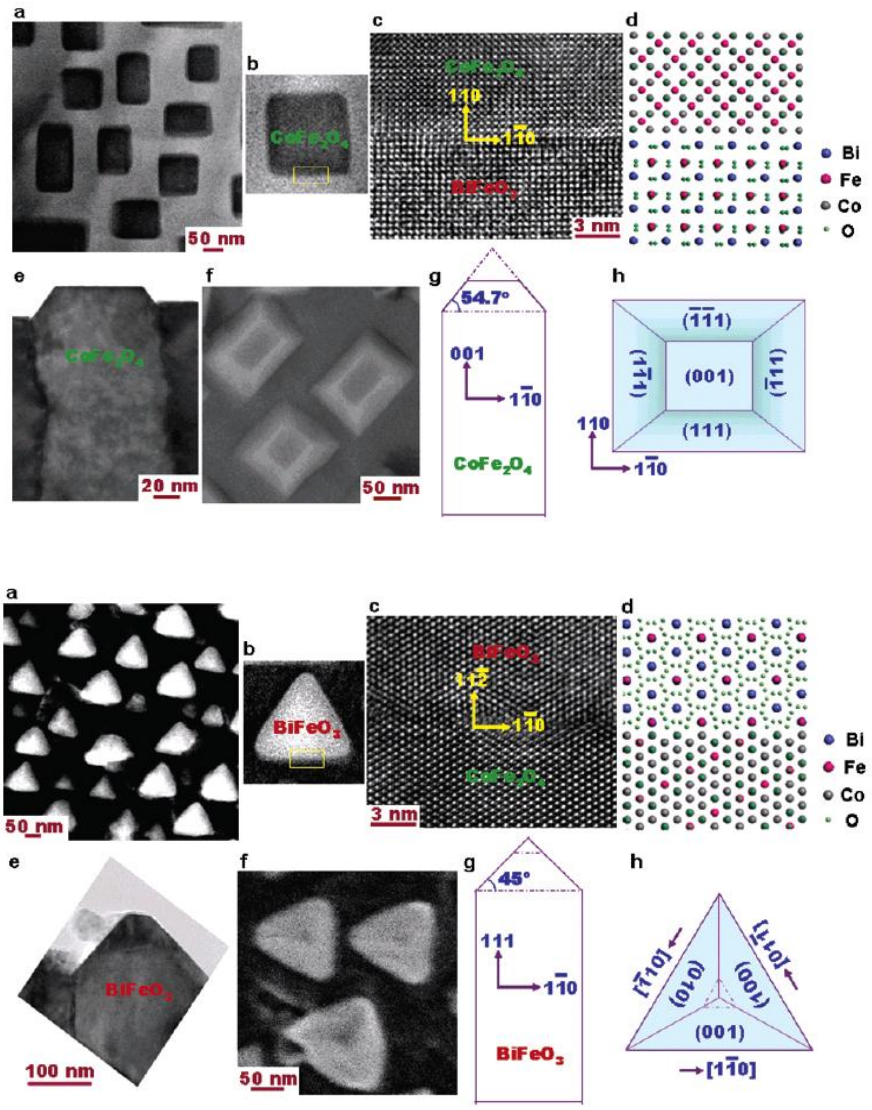

Figure 4. Morphologies of the $BiFeO_3$–$CoFe_2O_4$ nanostructures grown on a (001)-oriented (top) and a (111)-oriented (bottom) $SrTiO_3$ substrate. (a) Z-contrast image from a TEM sample. (b) A TEM image of a single $CoFe_2O_4$ pillar embedded in a $BiFeO_3$ matrix (top). A TEM image of a single $BiFeO_3$ pillar embedded in a $CoFe_2O_4$ matrix (bottom). (c) A high-resolution TEM image from the interface region marked by the rectangle in b. (d) Structural model of the interface between $CoFe_2O_4$ and $BiFeO_3$ showing that the interfaces are {110} planes (top) or {112} planes (bottom), both along ⟨110⟩ directions. (e) Cross-sectional TEM image of a single $CoFe_2O_4$ pillar (top) or $BiFeO_3$ pillar (bottom). (f) SEM image of the $CoFe_2O_4$ pillars (top) and $BiFeO_3$ pillars (bottom). (g) A schematic of a $CoFe_2O_4$ pillar (top) or a $BiFeO_3$ pillar (bottom). (h) A schematic of a $CoFe_2O_4$ pillar (top) or a $BiFeO_3$ pillar (bottom) showing three crystal facets. Figure from Ref [31] reprinted with permission from the American Chemical Society.

More morphologies of nanopillars based on rational selections of substrates have been demonstrated by Liao et al. [32]. They showed that in the $BiFeO_3$/$CoFe_2O_4$ system, $CoFe_2O_4$

nanopillars are in pyramid, roof, and triangular shapes on the (001), (011), and (111) surfaces, respectively (Figure 5). The magnetic anisotropies of these $CoFe_2O_4$ are different as well.

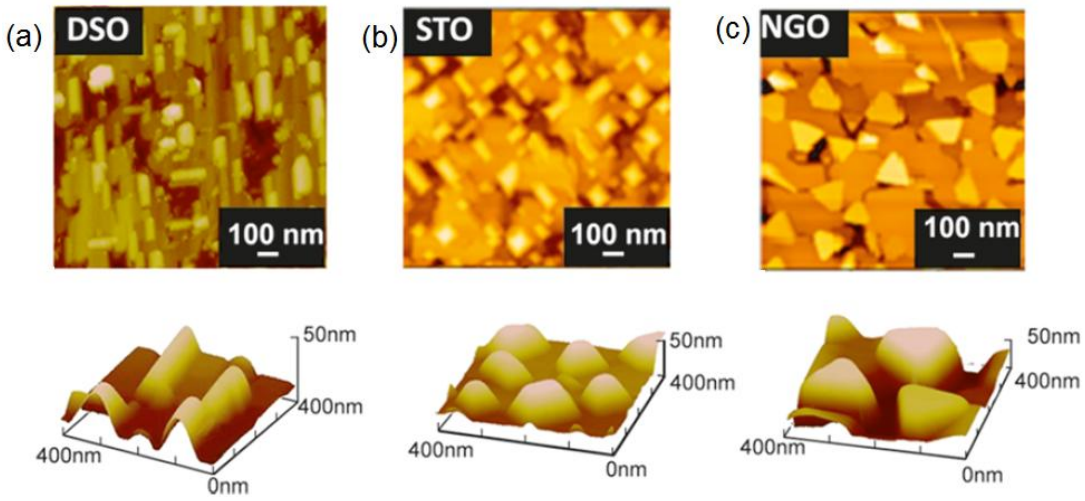

Figure 5. AFM topography of $BiFeO_3$–$CoFe_2O_4$ films. (a–c) 2D (3 μm × 3 μm) and 3D (500 nm × 500 nm) images of the films grown on different substrates. Figure from Ref [32] reprinted with permission from the American Chemical Society.

The substrates play a major role in the growth of the CA M nanopillars [21]. The density of the CA M hexagonal nanopillars was approximately 30 per μm^2 on a glass or silicon surface, which was much greater than the density of 0.1 per μm^2 found on the gold surface. The CA M nanopillars on a glass or silicon surface were shorter and smaller in diameter than those made on the gold surface.

In another work, Jayaramulu demonstrated that the surface of highly fluorinated graphene oxide (HFGO) had an orientation-directing property that guided the selective nucleation of zeolite imidazole framework (ZIF-8) nanostructures between HFGO layers. This HFGO/ZIF-8 composite may be used for separation of oil from water [33].

Other than substrate surfaces, factors to control the structure and subsequent properties of nanopillars include the following:

a) Vertical strain within layered heterostructures. It was recently shown that the vertical strain also controls the characteristics of the nanopillar films. Macmanus-Driscoll et al. [34] demonstrated that ordered nanostructures were produced from $La_{0.70}Sr_{0.3}MnO_3$/ZnO (LSMO/ZnO) and $BiFeO_3/Sm_2O_3$ (BFO/SmO) on a single-crystal $SrTiO_3$ (STO). Vertical strain dominated the strain state in the films. Yang et al. [35] suggested that the leakage current, the lattice parameters, the strain state of the two phases, and dielectric properties can be affected by the vertical interface. In another reports, Varanasi [36] and Zhu [37] showed that in $YBa_2Cu_3O_{7-x}$ (YBCO)/$BaSnO_3$ (BSO) nanocomposite thin films, the lattice BSO nanopillars was rather tuned by YBCO, but not the substrate.
b) Temperature. For example, the average diameter of $CoFe_2O_4$ pillars in a system were 9 and 70 nm at 750 and 950 ℃, respectively [17].
c) Deposition frequency. Chen et al. [38] observed that the morphology and properties of $(La_{0.7}Sr_{0.3}MnO_3)_{0.5}$:$(ZnO)_{0.5}$ (LSMO:ZnO) nanostructures on $SrTiO_3$ (STO) (001) substrates can be tuned with the deposition frequency.

d) Light. For instance, Liu et al. [39] demonstrated that light could induce a fast change in magnetization of self-assembled $CoFe_2O_4$ nanopillars in a photostrictive $SrRuO_3$ (SRO) film (Figure 6).

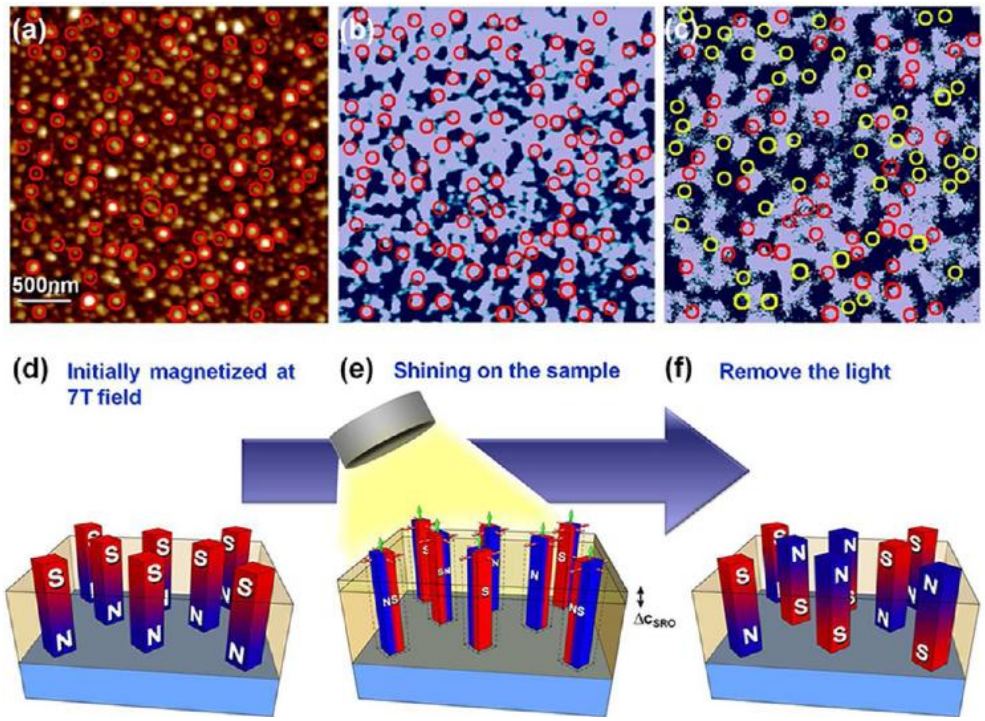

Figure 6. (a) AFM topology and (b) MFM image at the same area of a nanostructured CFO–SRO sample that has been magnetized by applying a large out-of-plane magnetic field before being illuminated. (c) MFM image at the same area after being illuminated. We randomly selected 100 nanopillars to conveniently observe the change in magnetic direction. The red circles in (b) are the nanopillars in (a) with downward magnetization, and half these pillars flipped upward in (c) are presented in yellow circles, suggesting a "liberation" in magnetization during illumination. (d–f) Schematic illustration of the process of magnetic domain flipping during the illumination by ultrafast Ti:sapphire laser pulses. (d) Application of a large out-of-plane magnetic field (7T) to magnetize all nanopillars downward. (e) Introduction of light on the nanostructured thin film to expand the lattice of SRO and release the vertical compressive strain of CFO. (f) Removal of light, resulting in the magnetization of the CFO nanopillars becoming either upward or downward for the energetically preferred state. Figure from Ref [39] reprinted with permission from the American Chemical Society.

4. Applications of the Self-assembled Nanopillars

Self-assembled vertical nanostructures have new functionalities. Some applications of these nanopillars are briefly summarized as follows:

4.1. Magnetoelectric

The nanopillar-embedded films hold potential as an excellent magnetoelectric materials. Magnetoelectric materials are materials that exhibit a coupling effect between the magnetic and the electric properties. The unique two-phase nanostructures that combine the vertically aligned nanopillars in a uniform film offers the potential to fabricating new magnetoelectric devices with stronger magnetoelectric responses.

Zheng et al. [13,17] prepared self-assembled epitaxial $CoFe_2O_4$–$BaTiO_3$ ferroelectromagnetic nanopillars on $SrTiO_3$ (001) substrates by using the pulsed laser deposition method (Figure 7). $CoFe_2O_4$ is magnetic and $BaTiO_3$ is ferroelectric. The size of the hexagonal $CoFe_2O_4$ nanopillars was from 20 to 30 nanometers. This nanocomposite showed strong magnetoelectric coupling.

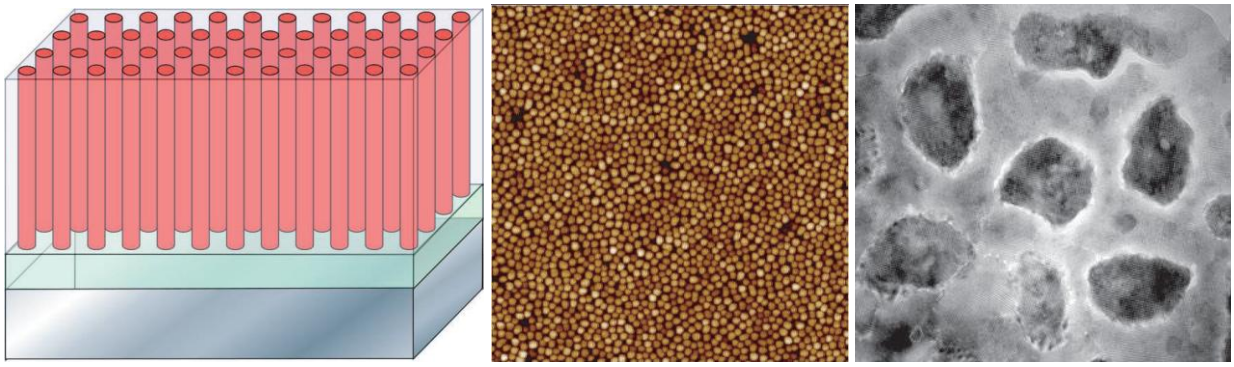

Figure 7. Left: Schematic illustration of a self-assembled nanostructured thin film formed on the substrate. Middle: AFM topography image of the film showing a quasi-hexagonal arrangement of the $CoFe_2O_4$ nanopillars. Right: TEM planar view image showing the $CoFe_2O_4$ nanostructures in the $BaTiO_3$ matrix. Figure from Ref [13] reprinted with permission from the AAAS.

Zavaliche et al. [40] also reported a similar epitaxial nanostructure with a thickness of ~200 nm. They presented direct evidence on magnetization reversal at room temperature. Stratulat et al. demonstrated a large area of highly ordered $CoFe_2O_4$-nanopillar/$BiFeO_3$ composite [41]. Further proof of enhanced ferromagnetic coupling can be found from Chen's work [42].

4.2. Ferroelectric

These nanopillar-embedded films may also be used as ferroelectric materials for energy harvesting to high-power electronic transducing. The ferroelectricity and ferroelectric Curie temperature *T*c can be affected from the strain in the oxide films.

In $BiFeO_3$:Sm_2O_3, an improvement in dielectric properties and reduced leakage were achieved when the vertical strain increased [34,35]. Harrington et al. [43] reported ferroelectric materials based on micrometer-thick films of $BaTiO_3$ (BTO), which were embedded with vertical pillars of Sm_2O_3 throughout the film (Figure 8). Sm_2O_3 is used to control the strain because 1) it does not dissolve in BTO; 2) its elastic modulus (125 GPa) is larger than that of BTO (67 GPa), and 3) it is an insulating material. The Curie temperature of the film was 330 ℃, and the phase transition

temperature was higher than 800 ℃, indicating it is a high-temperature ferroelectric material. The results also suggested that vertical nanopillars can be used to control strains in thicker films [44,45,46].

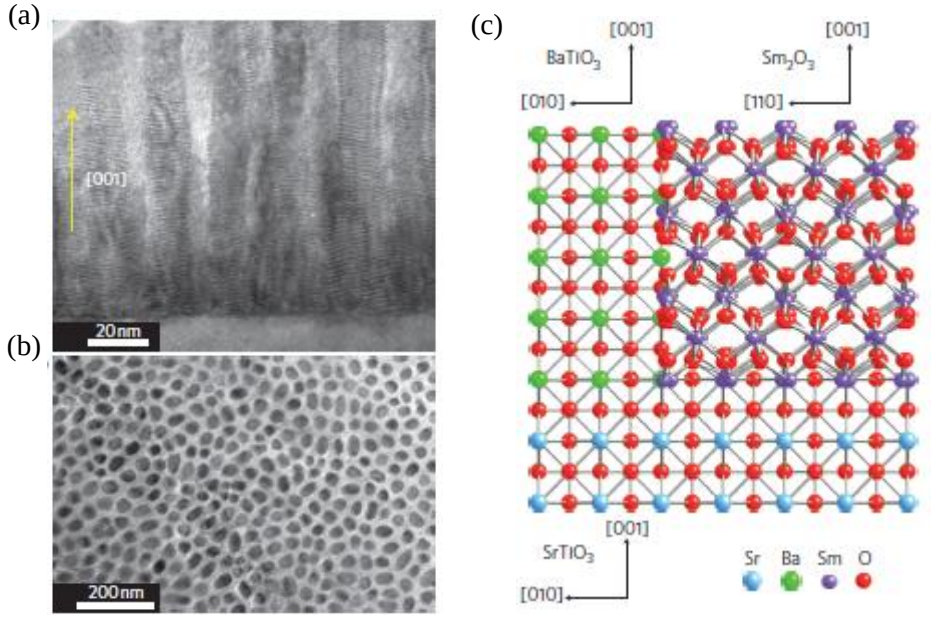

Figure 8. Self-assembled vertical nanostructure. TEM images of a 600-nm-thick $BaTiO_3$:Sm_2O_3 film on $SrTiO_3$: cross-section (a); plan view (b). Sm_2O_3 shows a darker contrast compared with $BaTiO_3$. Yellow arrow represents c-axis direction. (c) Crystallographic model of interface matching. Figure from Ref [43] reprinted with permission from the Nature Publishing Group.

4.3. Vortex Pinning and High Conductivity

The introduction of nanopillars in membranes may also be a promising approach for optimizing high-temperature superconductors (HTSs). This is due to an increase in their critical current density Jc and a reduction of their anisotropy. The introduction of nanostructures may pin magnetic flux vortices and oppose vortex motion induced by the Lorentz force.

Wee et al. prepared [47] Ba_2YNbO_6 (BYNO) nanopillars in $YBa_2Cu_3O_{7-\delta}$ (YBCO) films via a laser ablation method. The YBCO + BYNO films exhibited a superior Jc performance. Wee et al. [48] also reported another material with a structure of Ba_2RETaO_6.

Zhang et al. [30] reported a $BaFeO_2$ nanopillars-embedded superconducting $BaFe_2As_2$ thin film. The nanopillars provided effective flux pinning centers and high critical current density in the film (Figure 9). The use of self-assembled nanopillars as correlated defects for strong vortex pinning provides an efficient method for increasing Jc without any apparent film thickne0ss dependence or need for post-processing.

Several other pinning materials including Y_2BaCuO_5, $BaZrO_3$, $BaIrO_3$, Nd_2O_3, YSZ, Y_2O_3, and $BaSnO_3$ have also been investigated. Kang et al. [49] found that short segments of a superconducting wire and annopillar arrays in thicker films (3 μm) may be used for large-scale applications that require a high supercurrent.

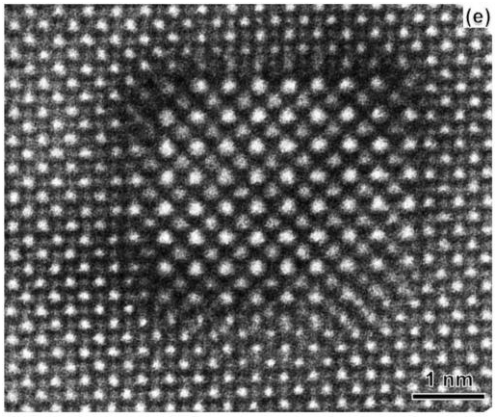

Figure 9. A high angle annular dark field (Z-contrast) image showing the atomic structure of an epitaxial nanopillar in the Ba-122 film. Figure from Ref [30] reprinted with permission from the American Chemical Society.

4.4. FET Spintronics

GaN-based quantum wells (QWs) are a promising candidate for optoelectronic devices, such as spin-polarized field effect transistors (spin-polarized FETs) [50]. When light-polarized M-plane GaN (Figure 10) and spin-polarized C-plane GaN are fabricated on the same substrate (e.g., γ-$LiAlO_2$), two-phase GaN provides an opportunity to combine optoelectronics and spintronics to an optically controlled spin-polarized FET by the coupling of polarized light and the polarized spin of 2DEG [51]. Hsieh et al. showed that the formation of GaN nanopillars is through nucleation on hexagonal anionic bases of $LiAlO_2$. This heterostructure might be used in optically controlled spintronic devices.

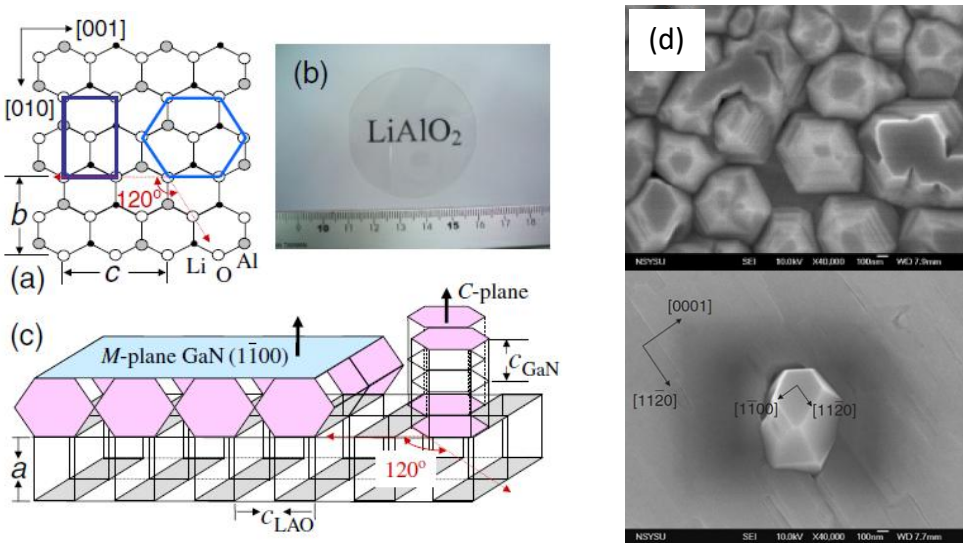

Figure 10. (a) Lattice structure of LAO (100). (b) High quality LAO wafer. (c) Schematic diagram of two-phase growth mode. (d) A 3D c-plane GaN nanopillar and a 2D M-plane GaN film are simultaneously grown on a γ-$LiAlO_2$ substate, forming a 120^o angle between them. Figure from Ref [51] reprinted with permission from the Japan Society of Applied Physics.

5. Conclusions

The self-assembled nanopillars hold great promises for developing novel electronic devices. The nanostructures can form over a large area, either as an array or embedded in a matrix, and the vertical interfaces have a significant effect on the property of the film. In a two-phase film, the materials exhibit coupling effect of the two materials. Investigations which are ongoing in this field include the optimization of ordered structures and the design of two-phase systems for better parameter coupling, such as metallic-nnaopillar/semiconductors [52] and metallic-nanopillars/ceramic composites [53]. More applications of the these structures are expected—for instance, recently, SRO/$SrTiO_3$ [54] and SRO/$Pb(Zr,Ti)O_3$ [55] were demonstrated to be photosensitive materials; Co-$BaZrO_3$ nanocomposite may be used for high density recording [56]. More applications in the energy field are expected. Furthermore, similar two phase systems have not been achieved in organic based materials since self-assembled nanopillars are still in their infancy. Realization of organic based two-phase, vertical nanocomposites may lead to new nanostructures with new electric or optical properties for multifunctional applications.

Conflict of Interest

The authors declare that there is no conflict of interest regarding the publication of this manuscript.

References

1. Fan Y, Ruebusch D, Rathore A, et al. (2009) Challenges and prospects of nanopillar-based solar cells. *Nano Res* 2: 829–843.
2. Fujii T, Aoki Y, Fushimi K, et al. (2010) Controlled morphology of aluminum alloy nanopillar films: form nanohorns to nanoplates. *Nanotechnology* 21: 395302.
3. Skupinski M, Johansson A, Jarmar T, et al. (2008) Carbon nanopillar array deposition on SiO_2 by ion irradiation through a porous alumina template. *Vacuum* 82: 359–362.
4. Park H, Kang M, Guo L (2009) Large area high density sub-20 nm SiO_2 nanostructures fabricated by bock copolymer template for nanoimprint lithography. *ACS Nano* 3: 2601–2608.
5. Liu J, Ashmkhan M, Wang B, et al. (2012) Fabrication and reflection properties of silicon nanopillars by cesium chloride self-assembly and dry etching. *Appl Surf Sci* 258: 8825–8830.
6. Liao Y, Liu J, Wang B (2012) Nanopillars by calcium chloride self-assembly and dry etching. *Mater Lett* 67: 323–326.
7. Keller F, Hunter F, Robinson D (1953) Structural features of oxide coatings on aluminum. *J Electrochem Soc* 100: 411–419.
8. Jessensky O, Muller F, Gosele U (1998) Self-organized formation of hexagonal pore arrays in anodic alumina. *Appl Phys Lett* 72: 1173–1175.
9. Schmidt-Grund R, Hilmer H, Hinkel A, et al. (2010) Two-dimensional confined photonic wire resonators—strong light-matter coupling. *Phys Status Solidi B* 247: 1351–1364.
10. Chen M, Yang J, Shiojiri M (2012) ZnO-based ultra-violet light emitting diodes and nanostructures fabricated by atomic layer deposition. *Semicond Sci Tech* 27: 074005.

11. Tiwary P, van de Walle A (2011) Hybrid deterministic and stochastic approach for efficient atomistic simulations at long time scales. *Phys Rev B* 84: 100301.
12. Logeeswaran V, Oh J, Nayak A, et al. (2011) A perspective on nanowire photodetectors: current status, future challenges, and opportunities. *IEEE J Sel Top Quant* 17: 1002–1032.
13. Zheng H, Wang J, Lofland S, et al. (2004) Multiferroic $BaTiO_3$–$CoFe_2O_4$ Nanostructures. *Science* 303: 661–663.
14. Ramesh R, Spaldin N (2007) Multiferroics: progress and prospects in thin films. *Nat Mater* 6: 21–29.
15. Lebedev O, Verbeeck J, Van Tendeloo G (2002) Structural phase transitions and stress accommodation in $(La_{0.67}Ca_{0.33}MnO_3)_{1-x}$:$(MgO)_x$ composite films. *Phys Rev B* 66: 104421.
16. Moshnyaga V, Damaschke B, Shapoval O, et al. (2003) Structural phase transition at the percolation threshold in epitaxial $(La_{0.7}Ca_{0.3}MnO_3)_{1-x}$:$(MgO)_x$ nanocomposite films. *Nat Mater* 2: 247–252.
17. Zheng H, Wang J, Mohaddes-Ardabili L, et al. (2004) Three-dimensional heteroepitaxy in self-assembled $BaTiO_3$–$CoFe_2O_4$ nanostructures. *Appl Phys Lett* 85: 2035–2037.
18. Li J, Levin I, Slutsker J, et al. (2005) Self-assembled multiferroic nanostructures in the $CoFe_2O_4$–$PbTiO_3$ system. *Appl Phys Lett* 87: 072909.
19. Levin I, Li J, Slutsker J, et al. (2006) Design of Self-Assembled Multiferroic Nanostructures in Epitaxial Films. *Adv Mater* 18: 2044–2047.
20. Roytburd A (1998) Thermodynamics of polydomain heterostructures. I. Effect of macrostresses. *J Appl Phys* 83: 228–238.
21. Deng Y, Zhou J, Wu D, et al. (2010) Three-dimensional phases-connectivity and strong magnetoelectric response of self-assembled feather-like $CoFe_2O_4$–$BaTiO_3$ nanostructures. *Chem Phys Lett* 96: 301–305.
22. Kim D, Sun X, Aimon N, et al. (2015) A Three Component Self-Assembled Epitaxial Nanocomposite Thin Film. *Adv Funct Mater* 25: 3091–3100.
23. Ji H, Xu X (2010) Hexagonal organic nanopillar array from the melamine-cyanuric acid complex. *Langmuir* 26: 4620–4622.
24. Seto C, Whitesides G (1993) Molecular self-assembly through hydrogen bonding: Supramolecular aggregates based on the cyanuric acid-melamine lattice. *J Am Chem Soc* 115: 905–916.
25. Kojtari A, Carroll P, Ji H (2014) Metal organic framework (MOF) micro/nanopillars. *CrystEngComm* 16: 2885–2888.
26. Kojtari A, Ji H (2015) Metal Organic Framework Micro/Nanopillars of Cu(BTC) $3H_2O$ and Zn(ADC) ĐDMSO. *Nanomaterials* 5: 565–576.
27. Hirade M, Nakanotani H, Yahiro M, et al. (2011) Formation of organic crystalline nanopillar arrays and their application to organic photovoltaic cells. *ACS Appl Mater Interfaces* 3: 80–83.
28. Ajiki Y, Kan T, Yahiro M, et al. (2016) Silicon based near infrared photodetector using self-assembled organic crystalline nano-pillars. *Appl Phys Lett* 108: 151102/1–151102/5.
29. Hu J, Luo Q, Zhang Z, et al. (2014) Self-assembled nanopillar arrays by simple spin coating from blending systems comprising PC61BM and conjugated polymers with special structure. *RSC Adv* 4: 24316–24319.
30. Zhang Y, Nelson C, Lee S, et al. (2011) Self-assembled oxide nanopillars in epitaxial $BaFe_2As_2$ thin films for vortex pinning. *Appl Phys Lett* 98: 042509.

31. Zheng H, Zhan Q, Zavaliche F, et al. (2006) Controlling Self-Assembled Perovskite–Spinel Nanostructures. *Nano Lett* 6: 1401–1407.
32. Liao S, Tsai P, Liang C, et al. (2011) Misorientation Control and Functionality Design of Nanopillars in Self-Assembled Perovskite–Spinel Heteroepitaxial Nanostructures. *ACS Nano* 5: 4118–4122.
33. Jayaramulu K, Datta K, Roesler C, et al. (2016) Biomimetic Superhydrophobic/Superoleophilic Highly Fluorinated Graphene Oxide and ZIF-8 Composites for Oil-Water Separation. *Angew Chem Int Ed* 55: 1178–1182.
34. Macmanus-Driscoll J, Zerrer P, Wang H, et al. (2008) Strain control and spontaneous phase ordering in vertical nanocomposite heteroepitaxial thin films. *Nat Mater* 7: 314–320.
35. Yang H, Wang H, Yoon J, et al. (2009) Vertical interface effect on the physical properties of self-assembled nanocomposite epitaxial films. *Adv Mater* 21: 3794–3798.
36. Varanasi C, Burke J, Brunke L, et al. (2007) Enhancement and angular dependence of transport critical current density in pulsed laser deposited $YBa_2Cu_3O_{7-x}$ + $BaSnO_3$ films in applied magnetic fields. *J Appl Phys* 102: 063909.
37. Zhu Y, Tsai C, Wang J, et al. (2012) Interfacial defects distribution and strain coupling in the vertically aligned nanocomposite $YBa_2Cu_3O_{7-x}$/$BaSnO_3$ thin films. *J Mater Res* 27: 1763–1769.
38. Chen A, Bi Z, Tsai C, et al. (2011) Tunable Low-Field Magnetoresistance in $(La_{0.7}Sr_{0.3}MnO_3)_{0.5}$:$(ZnO)_{0.5}$ Self-Assembled Vertically Aligned Nanocomposite Thin Film. *Adv Funct Mater* 21: 2423–2429.
39. Liu H, Chen L, He Q, et al. (2012) Epitaxial Photostriction Magnetostriction Coupled Self-Assembled Nanostructures. *ACS Nano* 6: 6952–6959.
40. Zavaliche F, Zheng H, Mohaddes-Ardabili L, et al. (2005) Electric Field-Induced Magnetization Switching in Epitaxial Columnar Nanostructures. *Nano Lett* 5: 1793–1796.
41. Stratulat S, Lu X, Morelli A, et al. (2013) Nucleation-Induced Self-Assembly of Multiferroic $BiFeO_3$–$CoFe_2O_4$ Nanocomposites. *Nano Lett* 13: 3884–3889.
42. Chen Y, Hsieh Y, Liao S, et al. (2013) Strong magnetic enhancement in self-assembled multiferroic–ferrimagnetic nanostructures. *Nanoscale* 5: 4449–4453.
43. Harrington S, Zhai J, Denev S, et al. (2011) Thick lead-free ferroelectric films with high Curie temperatures through nanocompositeinduced strain. *Nat Nanotechol* 6: 491–495.
44. Macmanus-Driscoll J, Foltyn S, Jia Q, et al. (2004) Strongly enhanced current densities in superconducting coated conductors of $YBa_2Cu_3O_{7-x}$ + $BaZrO_3$. *Nat Mater* 3: 439–443.
45. Aggarwal S, Monga A, Perusse S, et al. (2000) Spontaneous ordering of oxide nanostructures. *Science* 287: 2235–2237.
46. Fouchet A, Wang H, Yang H, et al. (2009) Spontaneous ordering, strain control, and multifunctionality in vertical nancomposite heteroepitaxial films. *IEEE T Ultrason Ferr* 56: 1534–1538.
47. Wee S, Goyal A, Zuev Y, et al. (2010) Formation of Self-Assembled, Double-Perovskite, Ba_2YNbO_6 Nanocolumns and Their Contribution to Flux-Pinning and Jc in Nb-Doped $YBa_2Cu_3O_{7-\delta}$ Films. *Appl Phys Exp* 3: 023101.
48. Wee S, Goyal A, Specht E, et al. (2010) Enhanced flux pinning and critical current density via incorporation of self-assembled rare-earth barium tantalate nanocolumns within $YBa_2Cu_3O_{7-\delta}$ films. *Phys Rev B* 81: 140503.

49. Kang S, Goyal A, Li J, et al. (2006) High-Performance High-Tc Superconducting Wires. *Science* 311: 1911–1914.
50. Lo I, Wang W, Gau M, et al. (2006) Gate-controlled spin splitting in GaN/AIN quantum wells. *Appl Phys Lett* 88: 082108.
51. Hsieh C, Lo I, Gau M, et al. (2008) Self-Assembled c-Plane GaN Nanopillars on γ-$LiAlO_2$ Substrate Grown by Plasma-Assisted Molecular-Beam Epitaxy. *Jpn J Appl Phys* 47: 891–895.
52. Kawasaki S, Takahashi R, Yamamoto T, et al. (2016) Photoelectrochemical water splitting enhanced by self-assembled metal nanopillars embedded in an oxide semiconductor photoelectrode. *Nat Commun* 7: 11818.
53. Su Q, Zhang W, Lu P, et al. (2016) Self-Assembled Magnetic Metallic Nanopillars in Ceramic Matrix with Anisotropic Magnetic and Electrical Transport Properties. *ACS Appl Mater Interfaces* 8: 20283–20291.
54. Schmising C, Harpoeth A, Zhavoronkov N, et al. (2008) Ultrafast Magnetostriction and Phonon-Mediated Stress in a Photoexcited Ferromagnet. *Phys Rev B* 78: 060404.
55. Schmising C, Bargheer M, Kiel M, et al. (2007) Coupled Ultrafast Lattice and Polarization Dynamics in Ferroelectric Nanolayers. *Phys Rev Lett* 98: 257601.
56. Huang J, Li L, Lu P, et al. (2017) Self-assembled Co-$BaZrO_3$ nanocomposite thin films with ultra-fine vertically aligned Co nanopillars. *Nanoscale* 9: 7970–7976.

AIMS Press

© 2017 Hai-Feng Ji, et al., licensee AIMS Press. This is an open access article distributed under the terms of the Creative Commons Attribution License (http://creativecommons.org/licenses/by/4.0)